

A Catalog of New M33 Star Clusters Based on the HST/WFPC2 Images

Won-Kee Park and Myung Gyoon Lee

*Astronomy Program, Department of Physics and Astronomy, Seoul National University,
Seoul 151-742, Korea*

wkpark@astro.snu.ac.kr, mglee@astrog.snu.ac.kr

ABSTRACT

We present the result of a survey for star clusters in M33 using the HST/WFPC2 archive images. We have found 104 star clusters, including 32 new ones, in the images of 24 fields that were not included in the previous studies. Combining these with previous data in the literature, we increase the number of M33 star clusters found in the HST images to 242. We have derived *BVI* integrated photometry of these star clusters from the CCD images taken with CFH12k mosaic camera at CFHT. Integrated color-magnitude diagrams of the M33 star clusters are found to be similar in general to those of star clusters in the Large Magellanic Cloud, except that M33 has a much lower fraction of blue star clusters. We find 29 red star clusters with $0.5 \leq (B - V)_0 \leq 1.1$ and $0.7 \leq (V - I)_0 \leq 1.2$, which are old globular cluster candidates. We divide the cluster sample into three groups according to their $(B - V)_0$ color: blue star clusters with $(B - V)_0 \leq 0.3$, intermediate color star clusters with $0.3 < (B - V)_0 < 0.5$, and red star clusters with $(B - V)_0 \geq 0.5$. Most of the new clusters in M33 are located along the sequence that is consistent with the theoretical evolutionary path for $Z = 0.004$, $Y = 0.24$ in the $(B - V)_0 - (V - I)_0$ diagram, while a few of them are in the redder side in the $(V - I)_0$ color. The red clusters are found relatively more in the outer region of M33 than the blue and intermediate color clusters, and that many of the blue stars are located in the HII regions. The luminosity function for the blue star clusters shows a peak at $M_V \approx -7.3$ mag, while that for the intermediate color star cluster shows a peak at the fainter magnitude $M_V \approx -6.3$ mag. The luminosity function for the red star clusters shows also a peak at $M_V \approx -6.8$ mag, although the number of the clusters is small.

Subject headings: galaxies: clusters — galaxies: individual (M33) — galaxies: photometry — galaxies: star clusters

1. Introduction

Star clusters are an important tool for understanding the formation and evolution of a galaxy. Being an aggregate of many stars, they are bright enough to be observed at great distances. They span a very broad range of age, from a few Myrs to more than 10 Gyrs, encapsulating the whole history of a galaxy. Age distribution of star clusters in a galaxy tells us about the formation and destruction history of the clusters and about the evolution of the galaxy as well. Spatial distribution of the star clusters delineates the structure of a galaxy, and their velocity distribution reveals the kinematics of stellar population and the mass of the host galaxy.

Recent studies for star clusters in nearby late type galaxies have revealed details of the star clusters, showing that the populations of star clusters are diverse among the galaxies (see Lee (2006) and references therein). Local Group galaxies in the nearby universe are ideal targets, due to their proximity, for studying in detail the properties of star clusters. There are three spiral galaxies in the Local Group: our Galaxy, M31 and M33. While star clusters in our Galaxy and M31 have been extensively studied, the star clusters in M33 received relatively less attention.

M33 (=NGC 598), the Triangulum galaxy, is a late type spiral galaxy (Scd). It is located at ~ 910 kpc from us (Kim et al. 2002). Its large angular size and inclination of $i = 56^\circ$ (Zaritsky et al. 1989) make it particularly suitable for studies of its stellar contents. Its mass, $M \sim 5 \times 10^{10} M_\odot$ (Corbelli 2003), falls in the intermediate range among the Local Group galaxies.

Surveys for star cluster in M33 have been rather sporadic. Early photometric surveys by Hiltner (1960) and Kron & Mayall (1960) identified about 25 star cluster candidates. Melnick & D’Odorico (1978) reported the discovery of 58 possible star cluster candidates, including most of the objects studied by Hiltner (1960). Christian & Schommer (1982) presented the most comprehensive catalog of 250 non-stellar objects in M33, including *BVR* photometry of 60 star cluster candidates. Later Christian & Schommer (1988) presented *BVI* photometry for 71 additional star cluster candidates. All these surveys were based on the photographic plates so that they were limited rather to the outer part of M33.

The first survey for M33 star clusters based on CCD imaging was given by Mochejska et al. (1998) using the *BVI* images from DIRECT project (Kaluzny et al. 1998; Stanek et al.

1998). They presented a list of 51 globular cluster candidates. While they covered the central region of M33 where previous surveys could not examine in detail, their survey was limited to the bright star clusters of $V \lesssim 19$ mag, and did not cover the entire area of M33.

The Hubble Space Telescope (HST) offers a great advantage over the ground-based telescopes for star cluster survey in M33. At the distance of M33, star clusters can be easily identified without ambiguity with HST images. Therefore, star cluster samples from HST images are much less likely to be contaminated by other extended sources such as a background galaxy or an H II region. Chandar et al. (1999a, 2001) searched for star clusters in M33 with HST data for the first time. They reported a discovery of 162 star clusters including 131 previously unknown ones in the 55 fields of HST/WFPC2 images. Recently, Bedin et al. (2005) have found 33 star clusters and 51 possible candidates from the $F775W(I)$ image of one HST/ACS field. Sarajedini et al. (2007) also reported a discovery of 24 star clusters including 11 new ones from the VI images of two HST/ACS fields in M33.

However, the areas of M33 covered by the previous HST-based surveys are much smaller than the entire area of M33. Therefore, it is needed to increase the number of HST fields to make as complete a sample of star clusters as possible. The sample of star clusters established from the HST images also serves as a template for ground-based star cluster surveys.

We searched for new M33 star clusters using the additional HST/WFPC2 images that became available after Chandar et al. (2001)'s work. We combined our result with previous M33 star cluster catalogs based on the HST images (Chandar et al. 1999a, 2001; Bedin et al. 2005; Sarajedini et al. 2007), and obtained homogeneous BVI photometry for the star clusters from the deep CCD imaging data taken at the Canada-France-Hawaii-Telescope (CFHT) (Park et al. 2007, in preparation)

In this paper, we present the result of M33 star cluster survey with the HST/WFPC2 images. Throughout this paper, we will refer the star clusters from the catalog of Bedin et al. (2005) with B designation, and ones from Chandar et al. (1999a, 2001) with CBF. CS designation means the star clusters from Christian & Schommer (1982, 1988), MKKSS designation means the ones from Mochejska et al. (1998), MD the ones from Melnick & D'Odorico (1978). Finally, SBGHS designation means the star clusters from Sarajedini et al. (2007).

The paper is composed as follows. Section 2 describes the HST/WFPC2 and CFHT data used in this study. In Section 3, star cluster search method and the integrated photometry procedures on CFHT images are described. Section 4 presents various properties of the star clusters: Color-magnitude diagrams (CMD), Color-color diagrams (CCD), and spatial distribution of star clusters. Finally, summary and conclusion are given in the last section.

2. Cluster Selection and Photometry

2.1. Cluster Selection

We used WFPC2 images of M33 in the HST archive that were not used in the previous studies by Chandar et al. (1999a, 2001). The images were obtained using various filter combinations of $F300W$, $F336W(U)$, $F436W(B)$, $F555W$, $F606W(V)$, and $F814W(I)$. We selected images only with exposure times longer than 100 sec either in V or I . The number of fields thus selected is 24, as listed in Table 1. The locations of the fields are displayed on Fig. 1, along with the locations of HST/WFPC2 fields for previous star cluster surveys (Chandar et al. 1999a, 2001). Nine of our fields are partially overlapped with previous survey regions. HST/WFPC2 image sets used by Chandar et al. (1999a, 2001) were also downloaded from the archive, and images of previously known star clusters on these image sets were utilized as references for the visual search on the new image sets.

Bright star clusters in M33 are easily resolved on the HST/WFPC2 images so that we selected star clusters using visual inspection of each image. We considered extended objects with the hint of resolved stars as star clusters.

Since the HST/WFPC2 image sets used in this study have different depths, and they cover different environments in M33 with different filters, we could not put a completeness limit of the survey for each image. The detection of star clusters depends not only on the brightness of the star clusters, but also on their sizes, morphologies, and environments. Experience from the visual investigation tells us that star clusters with $V \leq 20$ can be identified in the shallowest images of the current HST/WFPC2 image sets.

From the investigation of HST/WFPC2 fields, we have found 104 star clusters, 32 of which are new ones. The 32 new star clusters are listed in Table 2, and their V -band grayscale images are shown in Fig. 2. During the investigation, we identified eight CBF star clusters that were redundantly identified and registered under two different IDs: CBF-15 (CBF-45), CBF-20 (CBF-126), CBF-22 (CBF-91), CBF-53 (CBF-87), CBF-54 (CBF-85), CBF-56 (CBF-156), CBF-59 (CBF-95), and CBF-60 (CBF-94). The two star clusters in each pair have not only similar coordinates, but also similar V magnitudes with differences < 0.2 mag. We inspected carefully the HST/WFPC2 images of the regions where eight pairs are located, and we found neither two star clusters of similar magnitudes in the regions, nor any possible substructures (i.e. multiple OB groups in a cluster) in the clusters that Chandar et al. (1999a, 2001) might have recognized as two separate star clusters. Therefore, we regard these eight cases as redundant identifications of the same star cluster. Throughout this paper, we will present the total number of CBF samples as 154 instead of 162. From these 154 CBF samples, we identified 45 star clusters on our image sets.

One of our fields partially overlaps the region where Bedin et al. (2005) searched for star clusters with an HST/ACS image, where they found 33 star clusters and 51 star cluster candidates. 14 star clusters and 18 star cluster candidates fall on our HST/WFPC2 image. We could identify 13 star clusters except cluster ID 15 in Bedin et al. (2005)’s list that seems to be too faint to be seen on our $F606W$ image. We also inspected the 18 star cluster candidates on our image. However, they are so compact in size that it was impossible to tell whether they are star clusters, except for cluster ID 83 in Bedin et al. (2005)’s list. We classified this one as a star cluster after careful inspection of the image.

In addition, we found that 12 star cluster candidates from previous ground-based surveys (Christian & Schommer 1982; Mochejska et al. 1998; Melnick & D’Odorico 1978) are real star clusters. The coordinates, photometric properties, and cross identification among the various studies for these 71 previously known clusters are listed in Table 3.

We make a catalog of 242 star clusters in M33, combining our result with the previous results based on HST-based surveys (Chandar et al. 1999a, 2001; Bedin et al. 2005; Sarajedini et al. 2007). It is the largest catalog of M33 star clusters available to date which includes only the star clusters confirmed in the HST images. It consists of 32 newly found star clusters in this study, 12 previous star cluster candidates that were confirmed to be the genuine ones in this study, 154 star clusters from Chandar et al. (1999a, 2001), 32 star clusters out of 33 star clusters in Bedin et al. (2005), one star cluster from the star cluster candidate list of Bedin et al. (2005), and 11 new star clusters from the list of Sarajedini et al. (2007). The positions and the photometry of all M33 star clusters not included in Tables 2 and 3 are listed in Table 4.

2.2. Photometry

All star clusters in the combined catalog were observed with HST in different conditions with different purpose. The combination of the filters used for the HST observation varies depending on the field. To secure homogeneous photometry data for all clusters, we used the integrated photometry of these clusters derived from the ground-based images given in Park et al. (2007, in preparation) instead of deriving the photometry from the HST images.

Park et al. (2007) presented BVI integrated aperture photometry of clusters and cluster candidates in the $50' \times 80'$ field of M33 based on the CCD images taken with CFH12k mosaic camera at the Canada-France-Hawaii Telescope (CFHT). The typical seeing of the data is ~ 0.9 arcsec for all filters, and the point sources of $V \sim 23$ can be measured with errors smaller than 0.1. Details of the photometry are given in Park et al. (2007), and we give a

brief description here.

Examination of an aperture growth curve of isolated bright clusters on CFH12k CCD images indicates that most of star cluster light is contained within the aperture of $r \approx 4$ arcsec. However, using such an aperture would cause a large scatter in the measurement of some clusters, because star clusters are often located in the crowded field in M33 so that some neighbor objects happen to be inside the same aperture. For this reason, we used an aperture of $r = 2$ arcsec for the measurement of color, although the aperture of $r = 4$ arcsec was used for V magnitude measurement to measure the total light of the star clusters.

Some of the star clusters we missed happened to fall on the gaps between the chips in mosaic camera, and some of them happen to be located in so crowded a region that we could not derive their photometry from the CFHT images.

To supplement the photometry data for star clusters that could not be measured with CFH12k data, aperture photometry was carried out on the HST/WFPC2 images. We made photometry on the fields that were observed with more than two filters since instrumental magnitude cannot be converted to standard system without color information. For most of fields, two HST/WFPC2 images of identical pointings exist per filter. Fields observed with only one exposure were not included in the measurement. Two images were combined with COMBINE task in IRAF¹ with CRREJECT option to remove the cosmic rays. Cosmetic defects were masked with data quality images that accompany the scientific images. The centers of the clusters were determined visually with IRAF/IMEXAMINE task. Then IRAF/PHOT task was used to measure the instrumental magnitudes of star clusters on the combined images. To be consistent with previous HST-based studies (Chandar et al. 1999a, 2001; Sarajedini et al. 2007), aperture of $r = 2.2$ arcsec was adopted for the magnitude measurement, while aperture of $r = 1.0$ arcsec for color measurement. Local median values were measured as sky background level in the annulus of inner radius of $r = 3.5$ arcsec and outer radius of $r = 5.0$ arcsec around each star cluster. The CTE correction was applied to the instrumental magnitudes according to the prescription given at Dolphin (2002)'s web site². However, we did not correct for the geometrical distortions in the WFPC2 CCD. The instrumental magnitudes were converted to standard system using the relation also found at the same web site iteratively. In the end, we derived the photometry of 227 out of 242 star clusters with both CFH12k and HST/WFPC2 images.

¹IRAF is distributed by the National Optical Astronomy Observatories, which are operated by the Association of Universities for Research in Astronomy, Inc., under cooperative agreement with the National Science Foundation

²http://purcell.as.arizona.edu/wfpc2_calib/

We compared our photometry of the clusters with previous photometry. There are 154 clusters in common with Chandar et al. (1999a, 2001), 16 clusters in common with Christian & Schommer (1982), 12 clusters in common with Mochejska et al. (1998), and 11 clusters in common with Sarajedini et al. (2007). Note that all photometry was carried out with different aperture sizes: Chandar et al. (1999a, 2001) and Sarajedini et al. (2007) used nominal aperture of $r = 2.2$ arcsec for magnitude measurement, while Christian & Schommer (1982, 1988) used apertures of $r = 2.4$ and $r = 3.7$ arcsec, respectively. Mochejska et al. (1998) used an aperture of $r = 2.88$ arcsec. However, aperture sizes in all cases were determined to contain as much as possible the light from a star cluster, so the resultant aperture magnitudes for a star cluster should be more or less the same.

Fig. 3 shows the comparison of our photometry of the clusters with previous photometry. Large scatter made it difficult to see the difference in magnitude, but for bright star clusters ($V \leq 19$), there is little magnitude differences between this and other studies: $\Delta V(\text{this study-Chandar et al. (1999a, 2001)}) = -0.04$ with $\sigma = 0.19$, $\Delta V(\text{this study-Mochejska et al. (1998)}) = -0.04$ with $\sigma = 0.17$, $\Delta V(\text{this study-Christian \& Schommer (1982, 1988)}) = 0.00$ with $\sigma = 0.10$, and $\Delta V(\text{this study-Sarajedini et al. (2007)}) = -0.04$ with $\sigma = 0.12$, respectively. For fainter sources, however, our measurements get systematically fainter than the other space based measurements. Given that most of the star clusters are located in the region near the M33 center where crowding is severe and sky varies significantly, the sky background level was likely to be overestimated in ground-based images due to the unresolved faint stars, which would lead to a fainter estimation of source brightness.

Both the $(B - V)$ and $(V - I)$ colors show good agreement with all the previous studies down to the faintest magnitude in our samples. The differences between this study and other photometry are $\Delta(B - V)(\text{this study-Chandar et al. (1999a, 2001)}) = -0.05$ with $\sigma = 0.20$, $\Delta(V - I)(\text{this study-Chandar et al. (1999a, 2001)}) = -0.01$ with $\sigma = 0.10$, $\Delta(B - V)(\text{this study-Mochejska et al. (1998)}) = 0.06$ with $\sigma = 0.10$, $\Delta(V - I)(\text{this study-Mochejska et al. (1998)}) = 0.08$ with $\sigma = 0.22$, $\Delta(B - V)(\text{this study-Christian \& Schommer (1982, 1988)}) = 0.04$ with $\sigma = 0.08$, and $\Delta(V - I)(\text{this study-Sarajedini et al. (2007)}) = -0.04$ with $\sigma = 0.08$. The only exception to this tendency is the $(V - I)$ difference between ours and those of Christian & Schommer (1982, 1988), which turned out to be : $\Delta(V - I)(\text{this study-Christian \& Schommer (1982, 1988)}) = -0.16$ with $\sigma = 0.10$.

2.3. Reddening

To get the intrinsic color of the star clusters, the photometric measurements must be corrected for reddening. We estimated the foreground reddening for each star cluster using

the $(U - B)$ – $(B - V)$ diagram for early type stars in the field covering the cluster. We used the $UBVRI$ photometry of stars in the area of M33 covered in the Local Group Survey given by Massey et al. (2006). The $E(B - V)$ derived for each cluster is listed in the fourth column of Table 2, 3, and 4.

$E(B - V)$ values we derived for M33 star clusters range from ~ 0.05 to ~ 0.20 . For about 130 star clusters, the value of $E(B - V)$ turned out to be $E(B - V) = 0.1$, and for about 100 star clusters the values of $E(B - V)$ were found to be $E(B - V) \geq 0.15$. Chandar et al. (1999b) obtained $E(B - V)$ toward their 60 star clusters either from the photometry of neighboring individual stars by applying reddening free parameters or by using $E(B - V)$ values from Massey et al. (1995). The $E(B - V)$ values range $0.06 \sim 0.33$, and most of them are found to be 0.10. Sarajedini et al. (2000) also derived reddening for their 10 globular cluster samples from the shapes of the red giant branches (RGB) in the color-magnitude diagrams of resolved stars. Their $E(V - I)$ estimates are below 0.1, except for $E(V - I) = 0.25 \pm 0.03$ for Cluster ID 131 (=CS-H10). Sarajedini et al. (2007) also obtained $E(V - I)$ for 17 star clusters in the same way as Sarajedini et al. (2000), which $E(V - I)$ ranges from $0.10 \sim 0.45$.

Since our error in $E(B - V)$ measurement is as large as ~ 0.05 , it is quite difficult to see the consistency between our result and other results. But the fact that $E(B - V)$ distribution shows peak at $E(B - V) \sim 0.10$, a typical value found in previous studies (Chandar et al. 1999b), indicated that the result obtained in this study is in general consistent with previous studies.

3. Result

3.1. Color-magnitude diagram

Fig. 4 displays the integrated $M_V - (B - V)_0$ and $M_V - (V - I)_0$ color-magnitude diagrams (CMD) of the star clusters in M33. Absolute magnitudes of the star clusters were derived for the adopted distance modulus of $(m - M)_0 = 24.8$ (Kim et al. 2002) and the visual extinction to reddening ratio $R_V = 3.31$ (Schlegel et al. 1998). For comparison, we display the CMD for the star clusters in the LMC (Bica et al. 1996) in the panel (c), and the CMDs for the open clusters (Lata et al. 2002) and globular clusters (Harris 1996) in our Galaxy in panel (d). We adopted a value for the foreground reddening of $E(B - V) = 0.075$ (Schlegel et al. 1998) and the distance modulus of $(m - M)_0 = 18.5$ for the LMC clusters.

Several features are noted in Fig. 4. First, the star clusters in all three galaxies are roughly separated into blue and red groups with a color boundary of $(B - V)_0 \simeq 0.5$ in the

$M_V - (B - V)_0$ CMD. However, this separation for the M33 clusters in the $M_V - (V - I)_0$ CMD is not as clear as in the $M_V - (B - V)_0$ CMD. Second, the dominant population in M33 is blue clusters, as known before (Christian & Schommer 1982; Chandar et al. 1999b). Most of the new clusters found or the clusters confirmed in this study are also blue clusters. Third, the brightest blue clusters in M33 are as bright as $M_V \approx -9.0$ mag, which is similar to the value for the Galactic open clusters, but about 1.5 magnitude fainter than that for the LMC. Fourth, the blue envelope for the blue clusters in M33 in the $M_V - (B - V)_0$ CMD is slightly redder than that for the LMC blue clusters, as seen from the normalized $(B - V)_0$ color histograms in the panel (a) and (c). Fifth, there are only a small number of red clusters with $(B - V)_0 > 0.5$ in M33. The $(B - V)_0$ color range of the red clusters in M33, $0.5 < (B - V)_0 < 1.1$, is similar to that for the Galactic globular clusters, but is much larger than that for the LMC red clusters, $0.5 < (B - V)_0 < 0.8$. We found only one new red cluster, and confirmed two known red clusters. Cluster ID 85 (ID 27 in Mochejska et al. (1998)), one of the two red clusters confirmed in this study, happens to be the brightest ($M_V = -9.070$ and $(B - V)_0 = 0.575$) among the known red clusters in M33. The reddest cluster is cluster ID 89, which has integrated colors $(B - V)_0 = 1.579$, and $(V - I)_0 = 1.810$.

It is interesting to note that there are only a few red star clusters that are fainter than $M_V \sim -6.0$ in M33, while there are many such faint red star clusters seen in the LMC. The lack of faint red clusters in our catalog of M33 clusters may be due to incompleteness of our cluster search or may be an intrinsic feature of the M33 star cluster system. While we selected HST/WFPC2 images on the basis of V or I exposure times, many of resultant image sets were obtained with combinations of V and shorter wavelength passbands such as U and B , rather than the combinations of V and I . So there is a possibility that our star cluster detection might have been biased toward blue star clusters. However, it may be an intrinsic feature, considering that Chandar et al. (2001) already showed that M33 red star clusters with $(V - I)_0 > 0.78$ has log normal type luminosity function (LF), while intermediate color clusters with $(V - I)_0 \leq 0.78$ show no turnover down to the completeness limit in their LF.

3.2. Color-color diagram

Fig. 5 shows the integrated $(B - V)_0 - (V - I)_0$ color-color diagram (CCD) of M33 star clusters, along with $(B - V)_0$ and $(V - I)_0$ histograms of M33 star clusters. Galactic globular clusters are also plotted for comparison. We overlaid the theoretical evolutionary path for the Single Stellar Population (SSP) (Bruzual & Charlot 2003) for $Z = 0.004$, $Y = 0.24$ that was reported to give the best overall fit to their M33 star cluster samples which younger than $\log(t) \leq 9.0$ (Chandar et al. 1999b). For comparison, evolutionary path of SSP for $Z = 0.02$,

$Y = 0.28$ is also overlaid.

Most of the new clusters in M33 including the ones from Bedin et al. (2005) are located along the sequence that is consistent with the theoretical evolutionary path for $Z = 0.004$, $Y = 0.24$, while a few of them are in the redder side in the $(V - I)_0$ color. This is similar to the case of previously known clusters in M33 and also to the case of the star clusters in M51 (Hwang & Lee 2007). Some bright clusters among these redder clusters are consistent with the theoretical evolutionary path for $Z = 0.02$, $Y = 0.28$. However, the rest of them cannot be explained with any other models. The continuous distribution of star clusters along the model line indicates that M33 star clusters have been formed continuously from the epoch of the first star cluster formation until recent time.

The $(V - I)_0$ distribution shows only one peak at $(V - I)_0 = 0.45$ and monotonically decrease toward red end, while the $(B - V)_0$ distribution shows two distinct peaks at $(B - V)_0 \sim 0.15$ and $(B - V)_0 \sim 0.55$. The $(B - V)_0$ distribution is similar to that given by Sarajedini & Mancone (2007), except that the red peak at $(B - V)_0 \sim 0.55$ in our result, is 0.1 bluer than their result, $(B - V)_0 \sim 0.65$. The blue peak corresponds to the age of $\sim 2 \times 10^8$ year and the red one to the age of $\sim 1 \times 10^9$ year, if we assume the metallicity of the star clusters, $Z = 0.004$.

Based on the integrated photometry of the clusters, we can select old globular cluster candidates from our catalog. The $(B - V)_0$ color distribution shows the blue end of red star cluster population is located at $(B - V)_0 \sim 0.5$, which is similar to that of Galactic globular clusters. Although we do not see any similar red peak at $(V - I)_0$ color distribution of M33 star clusters, it is reasonable to set the color criterion for $(V - I)_0$ color as well, in accordance with the $(V - I)_0$ distribution of Galactic globular clusters. The color ranges for most of Galactic globular clusters in Fig. 5 are $0.5 \leq (B - V)_0 \leq 1.1$ and $0.7 \leq (V - I)_0 \leq 1.2$. There are 29 star clusters with this color range in our catalog, which are old globular cluster candidates in M33. Ten of them are newly found in this study. The globular cluster candidates are listed in Table. 5, along with their integrated photometry and cross identifications with previous catalogs.

Nine out of ten globular clusters in Sarajedini et al. (2000) satisfy our color selection criterion. One globular cluster, C38 in Christian & Schommer (1982) (=CBF-114), is not included because its color $(V - I)_0 = 0.684$ is a little bluer than the blue limit of the criterion. Our list of 29 globular cluster candidates also includes three oldest star clusters in the list of Sarajedini et al. (2007), clusters ID 58, 131, and 228 that are all estimated to be older than $\log(t) \sim 9.8$.

3.3. Spatial distribution

We divided the M33 star cluster sample into three groups according to their $(B - V)_0$ color for further analysis: blue star clusters with $(B - V)_0 \leq 0.3$, intermediate color star clusters with $0.3 < (B - V)_0 < 0.5$, and red star clusters with $(B - V)_0 \geq 0.5$. Fig. 6 displays the spatial distribution of each color group. We also plotted for comparison the locations of H II regions (Hodge et al. 1999) that trace well the spiral arm structures of M33. Since HST/WFPC2 observations covered in our catalog do not cover the entire area of M33, the spatial distribution of star clusters cannot be used for the study of spatial structure of the M33 cluster system. Fig. 6 shows that the red clusters are found relatively more in the outer region of M33 than the blue and intermediate color clusters, and that many of the blue stars are located in the HII regions.

Note the regions investigated in this study include three fields far east from M33 center (See Fig. 1 for locations of these fields.). Had any star clusters been found in these regions, it would give a clue on the extent of star cluster system in M33. However, no star clusters were found in these regions with our image sets.

3.4. Cluster luminosity function

With the largest sample of star clusters available, we derived the luminosity function (LF) of star clusters, displaying it in Fig. 7(a). Although we did not estimate the completeness of our survey, it appears that our survey is reasonably complete for clusters brighter than $V \leq 19$. Therefore, only the bright part of LF is considered in further discussion.

In Fig. 7(a) the LF for the blue star clusters shows a peak at $M_V \approx -7.3$ mag, and decreases as the magnitude gets fainter, while the intermediate color star cluster LF shows a peak at the fainter magnitude $M_V \approx -6.3$ mag. The LF for the red star clusters shows also a peak at $M_V \approx -6.8$ mag, although the number of the clusters is small.

We fitted the LFs for $V < 19$ mag using a single Gaussian function, obtaining $M_V(\text{peak}) = -6.90 \pm 0.04$ mag and $\sigma(M_V) = 1.96$ for the blue star clusters, $M_V(\text{peak}) = -6.34 \pm 0.05$ mag and $\sigma(M_V) = 1.53$ for the intermediate color star clusters, and $M_V(\text{peak}) = -6.79 \pm 0.06$ mag and $\sigma(M_V) = 1.39$ for the red star clusters.

Chandar et al. (2001) presented the LF of the M33 star clusters for two color groups: $0.70 < (V - I)_0 < 0.78$ (intermediate color star clusters) and $0.78 < (V - I)_0$ (red star clusters). So we derived the cluster LFs for the same color groups, as shown in Fig. 7(b). We also plotted the cluster LFs given by Chandar et al. (2001) in Fig. 7(c) for comparison.

We adjusted the LFs given by Chandar et al. (2001) applying the same distance modulus for M33 (we adopted $(m-M)_0 = 24.80$, while Chandar et al. (2001) adopted $(m-M)_0 = 24.64$), shifting the magnitude bins of Chandar et al. (2001)’s LF 0.16 magnitude brighter.

In Fig. 7(b) the LFs for the intermediate color and red star clusters derived according to the $(V - I)_0$ color show peaks at $M_V \approx -6.8$ mag, which is roughly similar to those derived according to the $(B - V)_0$ color in Fig. 7(a). However, the LFs for the intermediate color and red star clusters derived in this study are somewhat different from those given by Chandar et al. (2001) in Fig. 7(c). Our LFs contain a larger number of faint star clusters than those given by Chandar et al. (2001). The peak magnitude in the LF for the red star clusters derived in this study is about 0.3 magnitude fainter than that of Chandar et al. (2001), $M_V \approx -7.1$ mag, while the peak magnitude in the LF for the intermediate color star clusters in this study is similar to that of Chandar et al. (2001)’s, $M_V \approx -6.7$ mag.

Chandar et al. (2001) sampled brighter star clusters more than in our survey. Chandar et al. (2001) combined their catalog based on HST/WFPC2 data with the previous catalogs of M33 star clusters to increase the number of the sample for deriving the LFs. We used only star cluster samples obtained with HST observation. Previous ground based surveys covered a wider area in M33 with shallower depth and poorer resolution compared with the HST survey so that they would include preferentially a larger number of bright and large clusters than the HST surveys. For example, the blue LF for Bedin et al. (2005) samples included in this study with $(B - V)_0 \leq 0.3$ has a peak at the same magnitude to that for blue samples displayed in Fig. 7(a). Thus it is natural that our LFs include a higher portion of faint star clusters than those of Chandar et al. (2001).

4. Summary and Conclusion

We have carried out a survey of star clusters in M33 using the HST/WFPC2 images in the HST archive that were not covered in the previous studies. We have found 104 stars clusters including 32 new clusters and 12 known clusters confirmed in this study from 24 fields of HST/WFPC2 images. We combined 44 star clusters from this study, 154 star clusters from Chandar et al. (1999a, 2001), 33 star clusters from Bedin et al. (2005), and 11 star clusters from Sarajedini et al. (2007), to build a catalog of 242 star clusters. This is the most comprehensive catalog available to date which contains only the confirmed genuine star clusters in M33. We present the integrated photometry of these star clusters derived from the BVI images taken with the CFH12K CCD camera at the CFHT. Photometric properties of the star clusters are summarized as follows:

- The integrated color-magnitude diagram of star clusters shows that there are two distinct populations in M33: a large number of blue star clusters and a small number of red star clusters. The CMD of the M33 star clusters is in general similar to that of the LMC star clusters.
- We divide the cluster sample into three groups according to their $(B - V)_0$ color: blue star clusters with $(B - V)_0 \leq 0.3$, intermediate color star clusters with $0.3 < (B - V)_0 < 0.5$, and red star clusters with $(B - V)_0 \geq 0.5$. Most of the new clusters found or confirmed in this study are blue clusters. There are 29 old globular cluster candidates with $0.5 \leq (B - V)_0 \leq 1.1$ and $0.7 \leq (V - I)_0 \leq 1.2$, ten of which are newly found in this study.
- Most of the new clusters in M33 are located along the theoretical evolutionary path for $Z = 0.004$, $Y = 0.24$ in $(B - V)_0 - (V - I)_0$ color-color diagram, while a few of them are in the redder side in the $(V - I)_0$ color.
- The red clusters are found relatively more in the outer region of M33 than the blue and intermediate color clusters, and that many of the blue stars are located in the HII regions.
- The luminosity function (LF) for the blue star clusters shows a peak at $M_V \approx -7.3$ mag, while the intermediate color star cluster LF shows a peak at the fainter magnitude $M_V \approx -6.3$ mag. The LF for the red star clusters shows also a peak at $M_V \approx -6.8$, although the number of the clusters is small.

Authors thank Narae Hwang for many fruitful discussions and comments during the work in this study. This work was supported in part supported by the ABRL(R14-2002-058-01000-0). This is based in part on the W. -K. Park's Ph.D. thesis in Seoul National University.

REFERENCES

- Bedin, L. R., Piotto, G., Baume, G., Momany, Y., Carraro, G., Anderson, J., Messineo, M., & Ortolani, S. 2005, *A&A*, 444, 831
- Bica, E., Claria, J. J., Dottori, H., Santos, J. F. C., Jr., & Piatti, A. E. 1996, *ApJS*, 102, 57
- Bruzual, G., & Charlot, S. 2003, *MNRAS*, 344, 1000

- Chandar, R., Bianchi, L., & Ford, H. C. 1999a, *ApJS*, 122, 431
- Chandar, R., Bianchi, L., & Ford, H. C. 1999b, *ApJ*, 517, 668
- Chandar, R., Bianchi, L., & Ford, H. C. 2001, *A&A*, 366, 498
- Christian, C. A., & Schommer, R. A. 1982, *ApJS*, 49, 405
- Christian, C. A., & Schommer, R. A. 1988, *AJ*, 95, 704
- Corbelli, E. 2003, *MNRAS*, 342, 199
- Harris, W. E. 1996, *AJ*, 112, 1487
- Hiltner, W. A. 1960, *ApJ*, 131, 163
- Hodge, P. W., Balsley, J., Wyder, T. K., & Skelton, B. P. 1999, *PASP*, 111, 685
- Hwang, N., & Lee, M. G. 2007, *AJ*, submitted
- Kaluzny, J., Stanek, K. Z., Krockenberger, M., Sasselov, D. D., Tonry, J. L., & Mateo, M. 1998, *AJ*, 115, 1016
- Kim, M., Kim, E., Lee, M. G., Sarajedini, A., & Geisler, D. 2002, *AJ*, 123, 244
- Kron, G. E., & Mayall, N. U. 1960, *AJ*, 65, 581
- Lata, S., Pandey, A. K., Sagar, R., & Mohan, V. 2002, *A&A*, 388, 158
- Lee, M. G. 2006, *Bull. Astr. Soc. India*, 34, 99
- Ma, J., Zhou, X., Chen, J. -S., Wu, H., Jiang, Z. -J., Xue, S. -J., & Zhu, J. 2002, *Chinese J. Astron. Astrophys.*, 2, 197
- Massey, P., Armandroff, T. E., Pyke, R., Patel, K., & Wilson, C. 1995, *AJ*, 110, 2715
- Massey, P., Olsen, K. A. G., Hodge, P. W., Strong, S. B., Jacoby, G. H., Schlingman, W., & Smith, R. C. 2006, *AJ*, 131, 2478
- Melnick, J., & D’Odorico, S. 1978, *A&AS*, 34, 249
- Mochejska, B. J., Kaluzny, J., Krockenberger, M., Sasselov, D. D., & Stanek, K. Z. 1998, *Acta Astron.*, 48, 455
- Sarajedini, A., Geisler, D., Schommer, R., & Harding, P. 2000, *AJ*, 120, 2437

Sarajedini, A., Barker, M. K., Geisler, D., Harding, P., & Schommer, R. 2007, *AJ*, 133, 290

Sarajedini, A., & Mancone, C. L. 2007, *AJ*, 134, 447

Schlegel, D. J., Finkbeiner, D. P., & Davis, M. 1998, *ApJ*, 500, 525

Stanek, K. Z., Kaluzny, J., Krockenberger, M., Sasselov, D. D., Tonry, J. L., & Mateo, M.
1998, *AJ*, 115, 1894

Zaritsky, D., Elston, R., & Hill, J. M. 1989, *AJ*, 97, 97

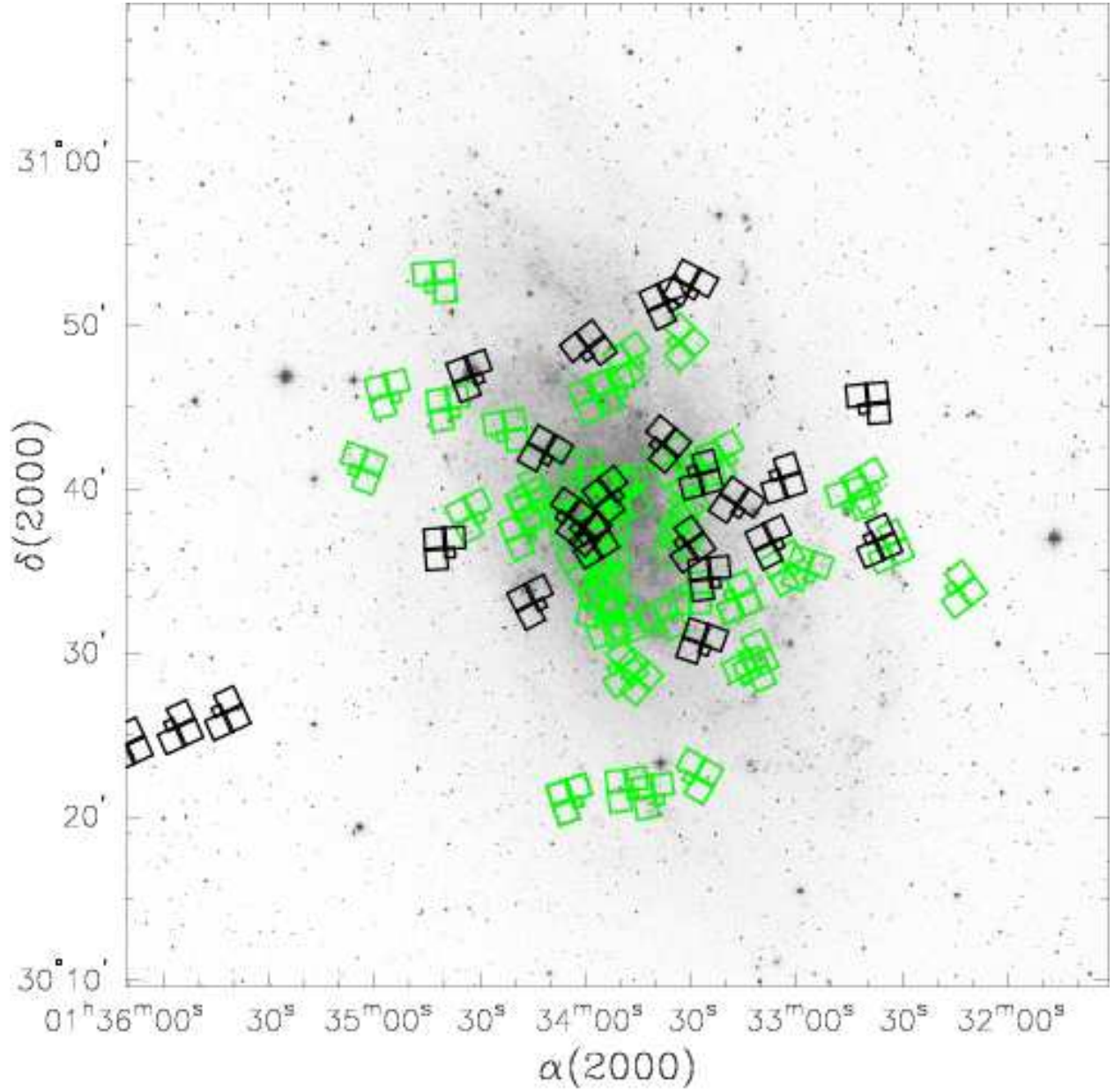


Fig. 1.— Locations of the HST/WFPC2 fields used in this study, overlaid in black on the grayscale map of $1^{\circ} \times 1^{\circ}$ Digitized Sky Survey image of M33. For comparison, locations of HST/WFPC2 fields for previous star cluster surveys (Chandar et al. 1999a, 2001) are shown in lighter tone.

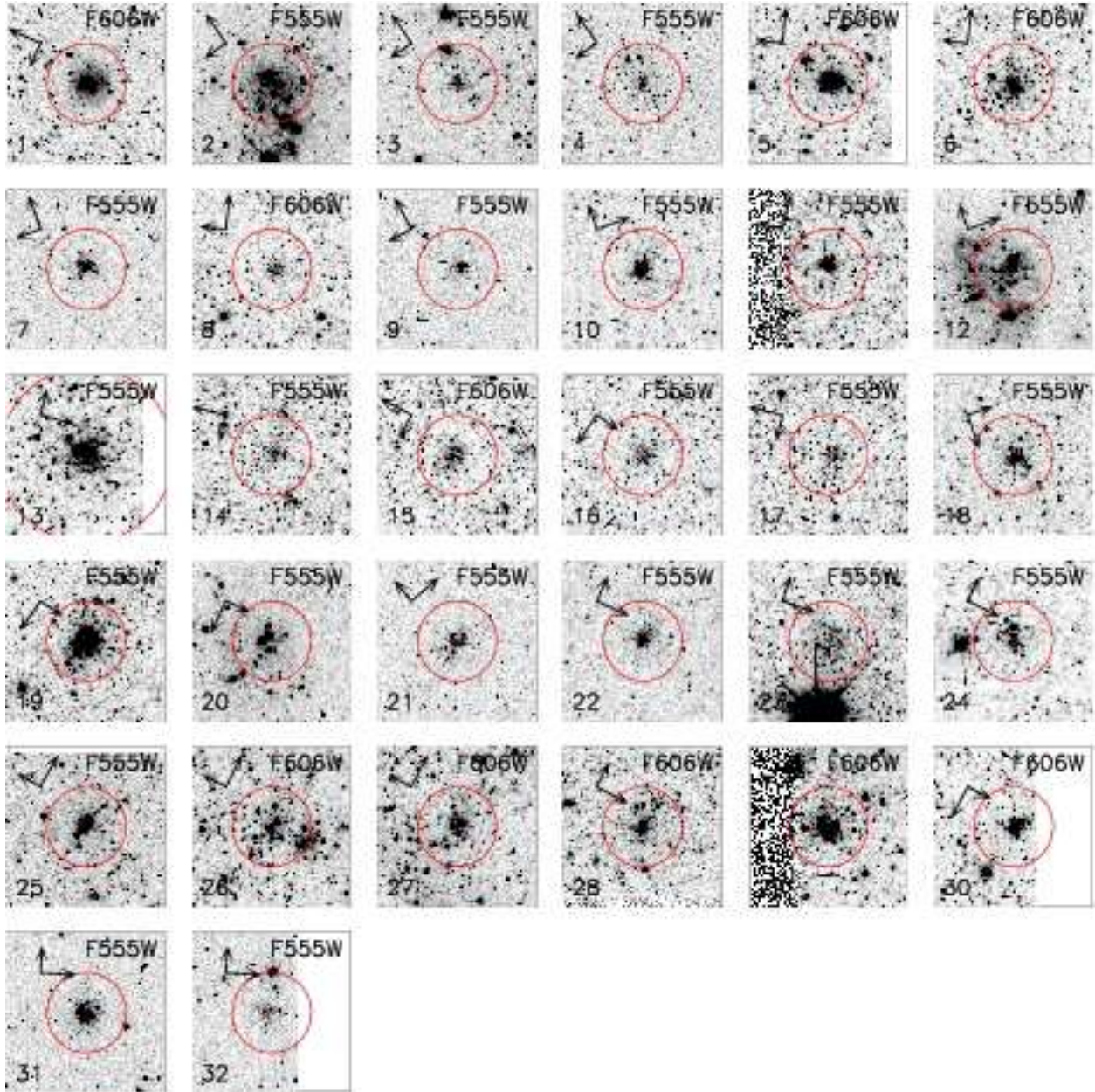


Fig. 2.— A mosaic of the grayscale maps of V band images of new M33 star clusters found in this study. A circle of $r = 3.0$ arcsec is drawn around the cluster to show the scale of each image. Longer and shorter arrows indicate, respectively, north and east. The labels in the right lower corner of each image represent the ID of each star cluster, and the ones in upper right corner the filter name of the each image.

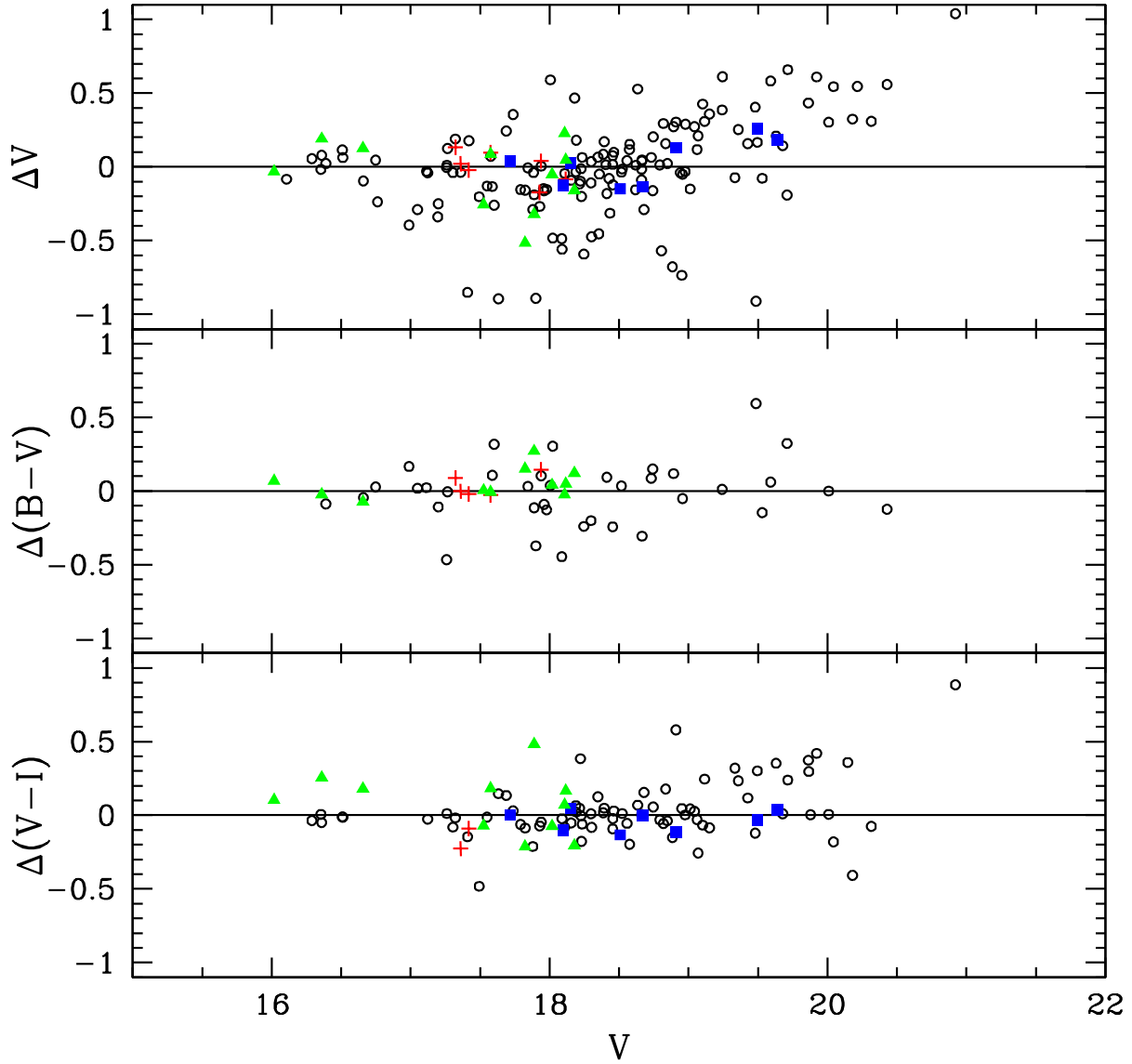


Fig. 3.— Comparison of the photometry between this study and previous studies. Open circles represent the photometry difference of Δ (this study - Chandar et al. (1999a, 2001)), filled squares the difference of Δ (this study - Sarajedini et al. (2007)), filled triangles Δ (this study - Mochejska et al. (1998)), and crosses denotes the difference of Δ (this study - Christian & Schommer (1982, 1988)).

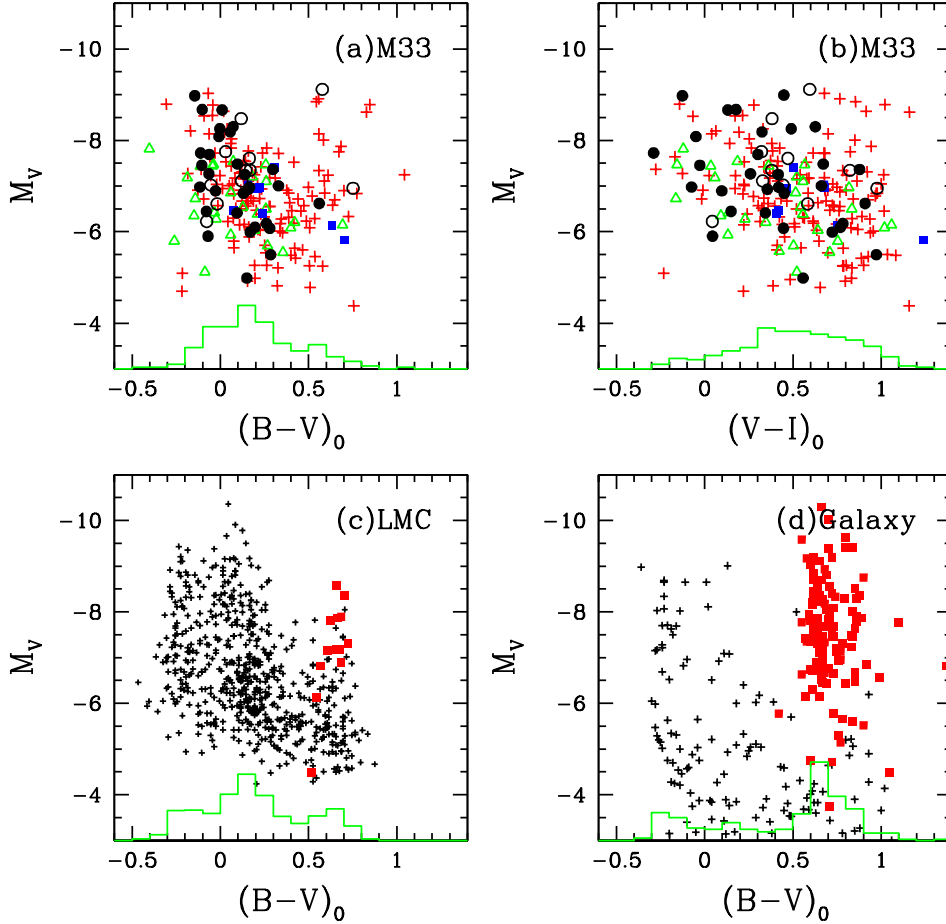


Fig. 4.— Integrated color-magnitude diagrams (CMD) of the star clusters in M33, Large Magellanic Cloud (LMC), and our Galaxy. Panels (a) and (b) show the $M_V-(B-V)_0$ CMD and the $M_V-(V-I)_0$ CMD of M33 star clusters, respectively. In both panels, filled circles denote the star clusters newly discovered in this study, and open circles denote the previously known star clusters that were confirmed in this study. Filled squares denote the star clusters from Sarajedini et al. (2007), Crosses the ones in the list of Chandar et al. (1999a, 2001), while triangles the star clusters from Bedin et al. (2005). Panel (c): integrated $M_V-(B-V)_0$ CMD of star clusters in the LMC (Bica et al. 1996). Panel (d): the integrated $M_V-(B-V)_0$ CMD of open clusters (Lata et al. 2002) and globular clusters (Harris 1996) in our Galaxy. Globular clusters are marked with filled squares in both panels. Histograms in all panels show the normalized distributions of colors for star cluster samples plotted in each panel.

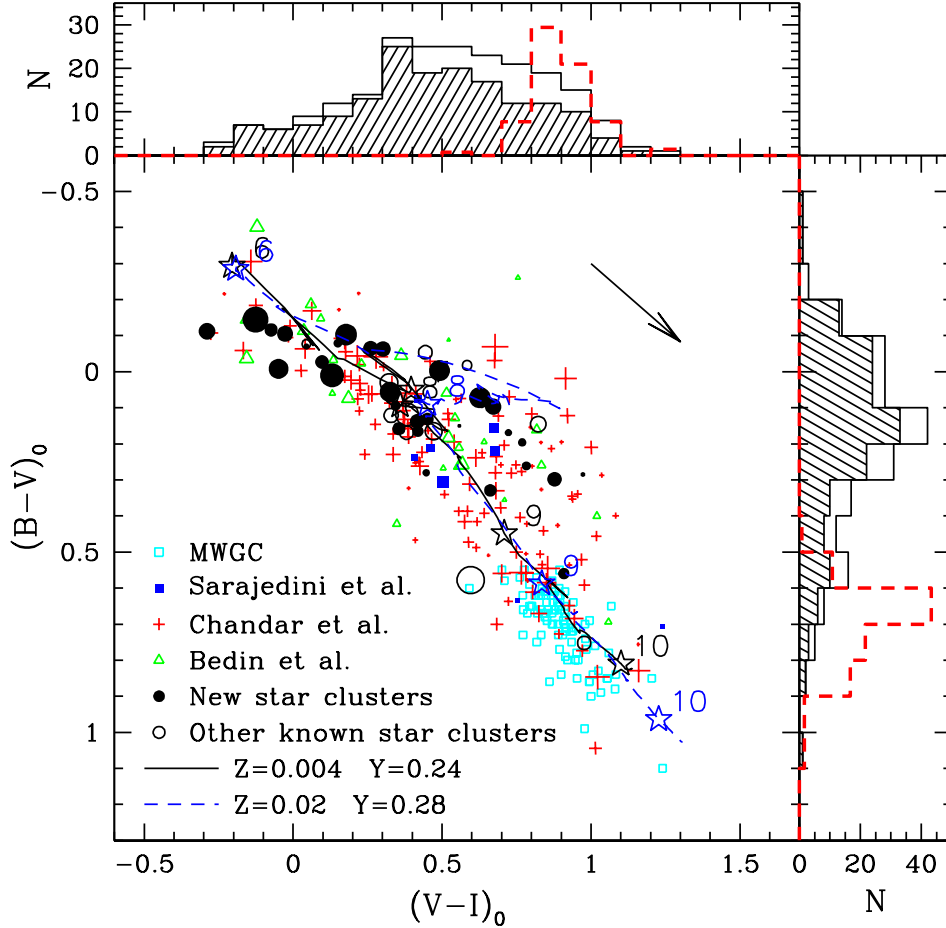


Fig. 5.— $(B - V)_0 - (V - I)_0$ diagram of the star clusters in M33. Same symbols are used for each group of star clusters as in panels (a) and (b) of Fig. 4. The sizes of symbols for M33 star clusters represent the relative brightness of the star cluster: the bigger, the brighter. Theoretical evolutionary paths from the Single Stellar Population (SSP) model (Bruzual & Charlot 2003) for $Z = 0.004$, $Y = 0.24$ (solid line), $Z = 0.02$, and $Y = 0.28$ (dashed line) are drawn with star symbols for every dex in age from 10^6 years to 10^{10} years. The arrow represents the reddening direction. Open histograms at upper and right side of the figure represent the distributions of the integrated colors for all M33 star clusters, while hatched histograms for star clusters brighter than $V \leq 19.0$. Color distributions of Galactic globular clusters are represented with dashed lines. Scales of Galactic globular cluster histograms are adjusted to fit in the figures.

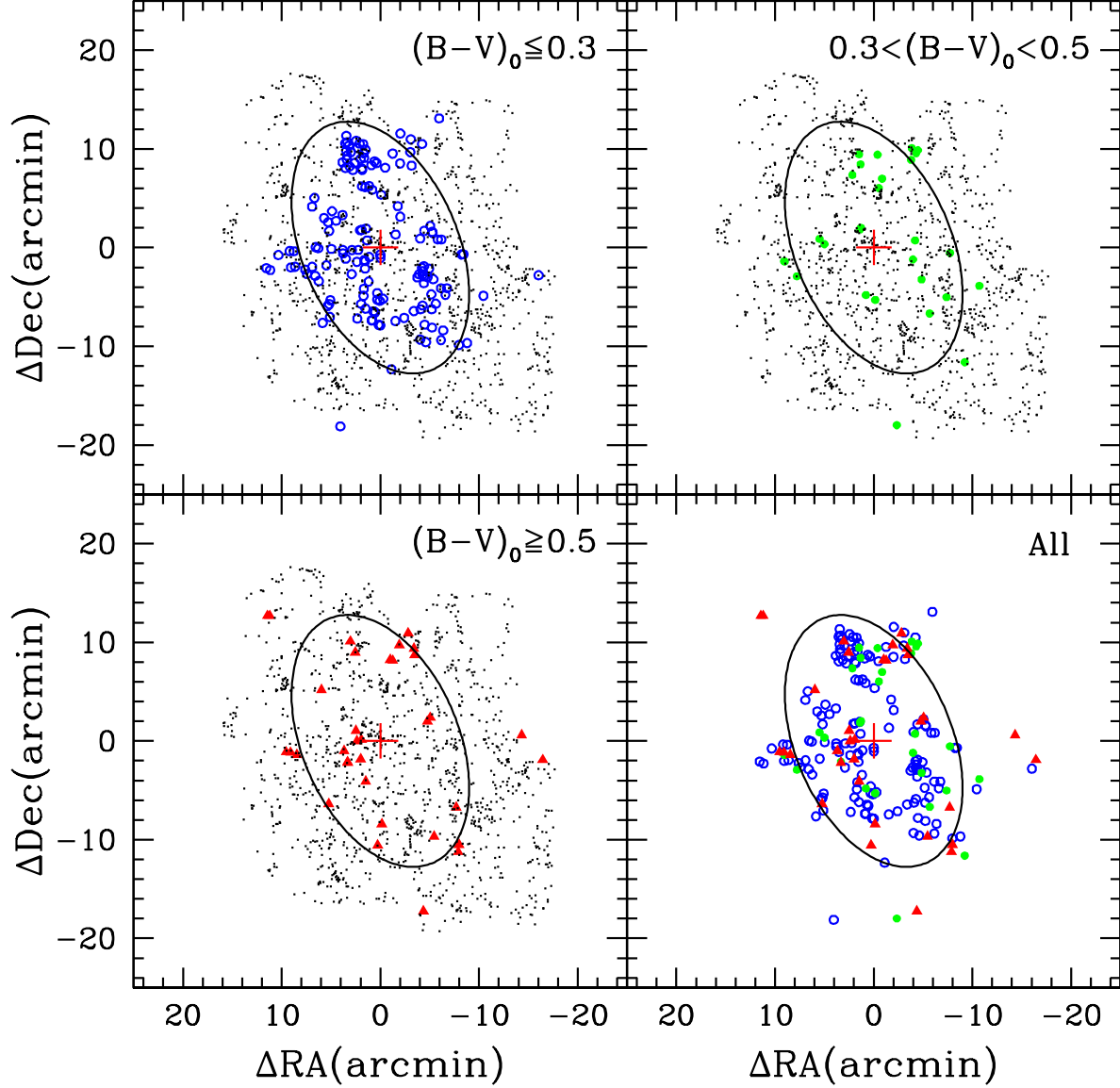


Fig. 6.— Spatial distribution of M33 star clusters: (a) blue star clusters with $(B-V)_0 \leq 0.3$, (b) intermediate color star clusters with $0.3 < (B-V)_0 < 0.5$, (c) red star clusters with $(B-V)_0 \geq 0.5$, and (d) all star clusters in our catalog. Small dots represent the locations of H II regions in M33 (Hodge et al. 1999). The center of M33 is marked with big plus sign. Schematic representation of M33 is shown on each panel by an ellipse with major axis length corresponding to the effective aperture (A_e) of M33.

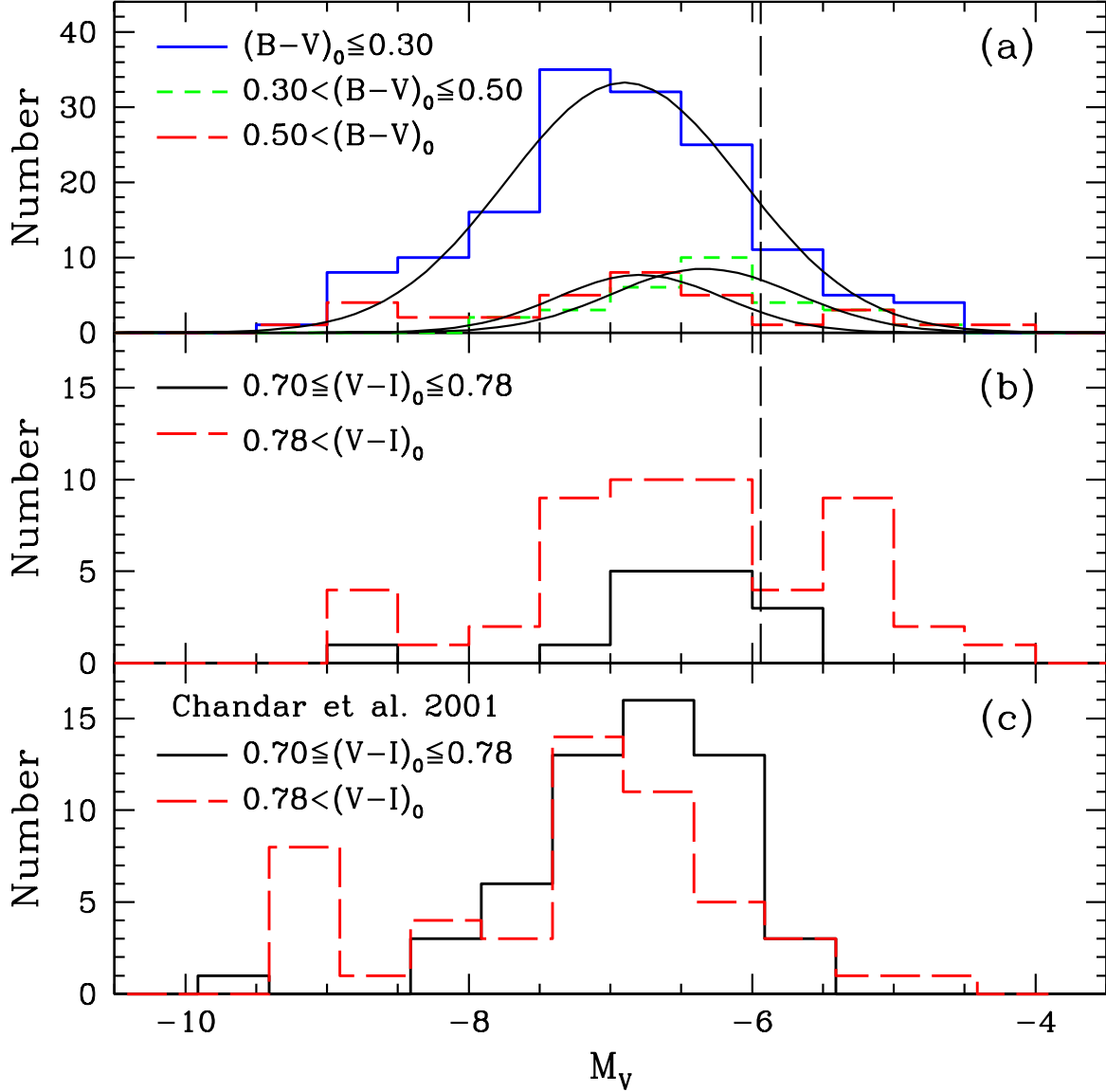


Fig. 7.— Luminosity function (LF) of M33 star clusters. (a) LFs for blue, intermediate color, and red star clusters that were classified according to their $(B - V)_0$ color. (b) LFs for intermediate color clusters and red clusters that were selected according to their $(V - I)_0$ color as used in Chandar et al. (2001). (c) LFs for intermediate color clusters and red clusters derived by Chandar et al. (2001), adjusted according to the distance modulus adopted in this study. Vertical dashed lines indicate roughly the cluster survey limit of this study.

Table 1. Summary of HST/WFPC2 fields used in this study

ID	PropID	Filters & Exposure Times				Number of Clusters
		$U(F336W)$	$B(F439W)$	$V(F505W)$	$I(F814W)$	new(all)
1	6694	$2 \times 800s^a$	$1 \times 500s$	$1 \times 100s$		0(8)
2	8805			$2 \times 700s^b$		2(6)
3	8207	$2 \times 400s$	$2 \times 300s$	$2 \times 120s$		1(10)
4	8207	$2 \times 400s$	$2 \times 300s$	$2 \times 120s$		3(7)
5	8207	$2 \times 400s$	$2 \times 300s$	$2 \times 120s$		1(5)
6	8805			$1 \times 1000s^b, 1 \times 900s^b$		0(5)
7	8018			$2 \times 1100s, 2 \times 800s$	$2 \times 1100s$	4(13)
8	6431		$2 \times 350s$	$2 \times 260s$	$1 \times 260s, 1 \times 200s$	5(13)
9	9127	$2 \times 260s$	$2 \times 300s$	$2 \times 160s$		3(0)
10	8805			$2 \times 700s^b$		3(6)
11	8805			$2 \times 700s^b$		6(7)
12	7909			$2 \times 500s^b$		0(17)
13	8207	$2 \times 400s$	$2 \times 300s$	$2 \times 120s$		0(0)
14	9127	$2 \times 260s$	$2 \times 300s$	$2 \times 160s$		4(7)
15	8207	$2 \times 400s$	$2 \times 300s$	$2 \times 120s$		2(0)
16	5237	$2 \times 600s$		$2 \times 200s$	$2 \times 200s$	0(0)
17	9127	$2 \times 160s, 2 \times 260s$	$2 \times 300s$	$2 \times 160s$		2(0)
18	8207	$2 \times 400s$	$2 \times 300s$	$2 \times 120s$		1(1)
19	8061	$1 \times 1600s^a$		$1 \times 700s^b$		1(1)
20	8207	$2 \times 400s$	$2 \times 300s$	$2 \times 120s$		0(0)
21	9479			$2 \times 140s^b$	$2 \times 500s$	0(0)
22	9127			$2 \times 140s^b$	$2 \times 500s$	0(0)
23	9127			$2 \times 140s^b$	$2 \times 500s$	0(0)
24	8207	$2 \times 400s$	$2 \times 300s$	$2 \times 120s$		0(0)

^aObserved with F300W.

^bObserved with F606W.

Table 2. Catalog of new M33 star clusters discovered in this study

ID	RA(2000)	Dec(2000)	V^a	$B - V^b$	$V - I^b$	$E(B - V)^c$
1	1 32 36.36	30 36 48.61	19.560 ± 0.012	0.130 ± 0.007	0.321 ± 0.015	0.20
2	1 33 11.74	30 38 56.14	$17.049 \pm 0.006^\dagger$	0.092 ± 0.008	0.089 ± 0.011	0.10
3	1 33 12.67	30 38 55.35	18.287 ± 0.027	0.231 ± 0.037	0.589 ± 0.037	0.10
4	1 33 14.97	30 39 04.70	18.291 ± 0.009	0.479 ± 0.009	0.869 ± 0.010	0.15
5	1 33 19.51	30 35 30.19	16.947 ± 0.003	0.156 ± 0.002	0.463 ± 0.004	0.10
6	1 33 20.25	30 34 50.27	17.677 ± 0.006	-0.005 ± 0.004	0.111 ± 0.009	0.10
7	1 33 21.35	30 31 13.02	18.719 ± 0.013	0.194 ± 0.008	0.482 ± 0.012	0.10
8	1 33 22.36	30 35 30.20	20.144 ± 0.056	0.250 ± 0.034	0.696 ± 0.052	0.10
9	1 33 23.15	30 52 42.41	19.220 ± 0.011	0.430 ± 0.009	0.654 ± 0.010	0.15
10	1 33 26.58	30 31 30.82	18.202 ± 0.010	0.258 ± 0.007	0.493 ± 0.010	0.10
11	1 33 27.38	30 41 48.39	19.017 ± 0.025	0.121 ± 0.018	0.426 ± 0.032	0.20
12	1 33 30.06	30 31 48.66	16.466 ± 0.002	0.110 ± 0.003	0.269 ± 0.004	0.10
13	1 33 30.23	30 41 18.89	18.489 ± 0.018	0.365 ± 0.013	0.695 ± 0.016	0.20
14	1 33 30.36	30 37 43.41	19.304 ± 0.039	0.319 ± 0.034	0.930 ± 0.040	0.15
15	1 33 30.38	30 36 41.45	19.034 ± 0.031	0.296 ± 0.022	0.907 ± 0.032	0.10
16	1 33 30.41	30 36 00.04	18.951 ± 0.028	0.361 ± 0.021	0.921 ± 0.026	0.10
17	1 33 31.32	30 37 34.10	19.798 ± 0.069	0.435 ± 0.040	1.180 ± 0.043	0.15
18	1 33 32.16	30 30 18.01	17.878 ± 0.006	0.238 ± 0.005	0.555 ± 0.006	0.10
19	1 33 32.46	30 35 38.30	16.308 ± 0.004	...	0.656 ± 0.004	0.15
20	1 33 36.54	30 50 35.79	17.574 ± 0.004	0.038 ± 0.004	-0.082 ± 0.009	0.15
21*	1 33 38.19	30 43 24.51	18.570 ± 0.012	0.739 ± 0.026	...	0.15
22	1 33 41.44	30 51 10.51	17.934 ± 0.058	0.448 ± 0.057	1.085 ± 0.076	0.15
23	1 33 58.09	30 37 29.68	17.771 ± 0.013	0.137 ± 0.015	0.578 ± 0.022	0.20
24	1 33 58.49	30 38 20.96	16.790 ± 0.005	0.097 ± 0.006	0.454 ± 0.013	0.20
25	1 33 58.67	30 35 26.10	16.156 ± 0.007	-0.045 ± 0.005	0.012 ± 0.009	0.10
26	1 34 14.44	30 34 17.56	16.879 ± 0.013	0.097 ± 0.013	0.629 ± 0.016	0.10
27	1 34 14.96	30 33 53.66	17.864 ± 0.013	0.035 ± 0.011	0.398 ± 0.015	0.10
28	1 34 15.21	30 33 15.11	18.512 ± 0.014	0.660 ± 0.014	1.047 ± 0.012	0.10
29	1 34 15.74	30 33 41.02	16.834 ± 0.011	0.172 ± 0.011	0.765 ± 0.012	0.10
30	1 34 18.08	30 31 58.93	18.154 ± 0.006	-0.016 ± 0.005	0.064 ± 0.012	0.10
31	1 34 42.79	30 37 20.21	17.652 ± 0.003	0.197 ± 0.002	0.810 ± 0.003	0.10
32	1 34 44.60	30 37 32.32	18.071 ± 0.005	0.023 ± 0.009	0.166 ± 0.015	0.05

^aMeasured on CFH12k CCD image with $r = 4.0''$ aperture.

^bMeasured on CFH12k CCD image with $r = 2.0''$ aperture.

^cMeasured with *UBVRI* PSF Photometry data by Massey et al. (2006). The uncertainties of the values are 0.05.

[†]Happened to be very close to the edge of the CCD chip. So the measurement was made with smaller apertures.

*Measured on HST/WFPC2 image instead of CFH12k CCD image, with $r = 2.2''$ and $r = 1.0''$ apertures for V and color measurement, respectively.

Table 3. Catalog of previously known M33 star clusters confirmed in this study

ID	RA(2000)	Dec(2000)	V^a	$B - V^b$	$V - I^b$	$E(B - V)^c$	Cross Identification ^d
33	1 32 34.45	30 37 42.09	20.180 ± 0.019	0.559 ± 0.016	0.725 ± 0.020	0.05	CBF-143
34	1 33 22.12	30 40 26.15	18.090 ± 0.010	0.080 ± 0.007	0.360 ± 0.014	0.10	CBF-59
35	1 33 22.26	30 40 59.64	18.663 ± 0.017	... *	0.475 ± 0.018	0.10	CBF-60
36	1 33 22.35	30 30 14.67	17.378 ± 0.004	0.130 ± 0.002	0.460 ± 0.004	0.10	CS-H36
37	1 33 23.84	30 40 26.18	19.480 ± 0.040	0.177 ± 0.026	0.685 ± 0.041	0.10	CBF-96
38	1 33 24.81	30 33 55.25	20.429 ± 0.077	-0.117 ± 0.032	0.358 ± 0.068	0.10	CBF-18
39	1 33 25.60	30 29 57.03	18.179 ± 0.006	0.852 ± 0.005	1.115 ± 0.004	0.10	CS-U126, MKKSS-5
40	1 33 25.96	30 36 24.58	17.525 ± 0.007	0.265 ± 0.005	0.610 ± 0.007	0.10	MKKSS-6
41	1 33 26.34	30 41 06.96	18.909 ± 0.021	0.477 ± 0.014	1.043 ± 0.016	0.20	CBF-92
42	1 33 26.46	30 41 11.84	19.358 ± 0.028	0.361 ± 0.022	0.786 ± 0.031	0.20	CBF-93

^aMeasured on CFH12k CCD image with $r = 4.0''$ aperture.

^bMeasured on CFH12k CCD image with $r = 2.0''$ aperture.

^cMeasured with *UBVRI* PSF Photometry data by Massey et al. (2006). The uncertainties of the values are 0.05.

^dB identifications are from Bedin et al. (2005); CBF identifications from Chandar et al. (1999a, 2001); CS identification from Christian & Schommer (1982); MKKSS identifications from Mochejska et al. (1998); MD identifications are from Melnick & D’Odorico (1978) based on the coordinates given by Ma et al. (2002) ; and S identifications from Sarajedini et al. (2007).

*Happened to be off from CFHT CFH12k images.

Note. — The complete version of this table is in the electronic edition of the Journal. The printed edition contains only a sample.

Table 4. Catalog of previously known M33 star clusters

ID	RA(2000)	Dec(2000)	V^a	$B - V^b$	$V - I^b$	$E(B - V)^c$	Cross Identification ^d
105*	1 32 38.83	30 39 17.77	19.942 ± 0.065	0.267 ± 0.090	...	0.10	CBF-162
106	1 32 44.28	30 40 12.25	18.434 ± 0.005	0.749 ± 0.006	1.065 ± 0.006	0.10	CBF-161, CS-U88
107	1 33 01.16	30 35 44.65	19.485 ± 0.026	0.449 ± 0.029	1.152 ± 0.028	0.05	CBF-39
108	1 33 02.39	30 34 44.16	18.022 ± 0.006	-0.034 ± 0.004	0.082 ± 0.011	0.15	CBF-40
109	1 33 08.10	30 28 00.12	19.062 ± 0.015	0.638 ± 0.011	0.822 ± 0.013	0.15	CBF-86, CS-U140
110	1 33 10.08	30 29 56.51	18.523 ± 0.022	0.296 ± 0.016	0.483 ± 0.018	0.15	CBF-89
111	1 33 13.84	30 29 05.27	18.884 ± 0.013	0.837 ± 0.014	0.999 ± 0.015	0.20	CBF-53
112	1 33 13.88	30 29 44.87	17.929 ± 0.012	0.042 ± 0.013	-0.069 ± 0.018	0.15	CBF-88
113	1 33 14.28	30 28 22.78	18.298 ± 0.006	0.874 ± 0.005	1.109 ± 0.004	0.10	CBF-54, CS-U137, MD-8
114	1 33 15.15	30 32 53.26	19.714 ± 0.026	0.629 ± 0.018	0.856 ± 0.018	0.05	CBF-144

^aMeasured on CFH12k CCD image with $r = 4.0''$ aperture.

^bMeasured on CFH12k CCD image with $r = 2.0''$ aperture.

^cMeasured with *UBVRI* PSF Photometry data by Massey et al. (2006). The uncertainties of the values are 0.05.

^dB identifications are from Bedin et al. (2005); CBF identifications from Chandar et al. (1999a, 2001); CS identification from Christian & Schommer (1982); MKKSS identifications from Mochejska et al. (1998); MD identifications are from Melnick & D’Odorico (1978) based on the coordinates given by Ma et al. (2002); and S identifications from Sarajedini et al. (2007).

*Measured on HST/WFPC2 image instead of CFH12k CCD image, with $r = 2.2''$ and $r = 1.0''$ apertures for V and color measurement, respectively.

Note. — The complete version of this table is in the electronic edition of the Journal. The printed edition contains only a sample.

Table 5. List of globular cluster candidates

ID	V^a	$B - V^b$	$V - I^b$	$E(B - V)^c$	Cross Identification ^d
28	18.512 ± 0.014	0.660 ± 0.014	1.047 ± 0.012	0.10	
39	18.179 ± 0.006	0.852 ± 0.005	1.115 ± 0.004	0.10	CS-U126, MKKSS-5
45	18.348 ± 0.011	0.789 ± 0.009	1.140 ± 0.009	0.20	CBF-90, CS-U77, MD-17
49	17.322 ± 0.006	0.759 ± 0.005	0.976 ± 0.004	0.20	CBF-90
58	19.497 ± 0.011	0.885 ± 0.015	1.098 ± 0.015	0.25	SBGHS-10
76	17.889 ± 0.016	0.711 ± 0.018	0.942 ± 0.013	0.10	CBF-49, MKKSS-25
84	18.454 ± 0.034	0.742 ± 0.050	1.185 ± 0.040	0.15	CBF-29
93	17.791 ± 0.009	0.658 ± 0.009	0.920 ± 0.011	0.10	CBF-118
94	18.155 ± 0.011	0.600 ± 0.011	0.888 ± 0.014	0.10	CBF-119
106	18.434 ± 0.005	0.749 ± 0.006	1.065 ± 0.006	0.10	CBF-161, CS-U88
111	18.884 ± 0.013	0.837 ± 0.014	0.999 ± 0.015	0.20	CBF-53
113	18.298 ± 0.006	0.874 ± 0.005	1.109 ± 0.004	0.10	CBF-54, CS-U137, MD-8
114	19.714 ± 0.026	0.629 ± 0.018	0.856 ± 0.018	0.05	CBF-144
130	19.012 ± 0.013	0.685 ± 0.013	1.043 ± 0.013	0.15	CBF-108, SBGHS-6
131	18.215 ± 0.006	1.244 ± 0.007	1.291 ± 0.005	0.20	CBF-106, SBGHS-4
146	16.290 ± 0.002	0.645 ± 0.001	0.993 ± 0.001	0.10	CBF-61, CS-U49, MD-24, MKKSS-21
149	19.042 ± 0.021	0.606 ± 0.016	0.967 ± 0.013	0.10	CBF-62
157	19.878 ± 0.053	0.605 ± 0.063	0.920 ± 0.068	0.10	CBF-138
163	17.261 ± 0.003	0.784 ± 0.003	1.082 ± 0.003	0.10	CBF-104, CS-H38, MD-25, MKKSS-22
189	16.390 ± 0.003	0.707 ± 0.002	0.973 ± 0.002	0.15	CBF-28
191	16.512 ± 0.008	0.929 ± 0.007	1.298 ± 0.005	0.10	CBF-98, MKKSS-31
196	19.149 ± 0.018	0.844 ± 0.029	1.266 ± 0.022	0.15	B-5
206	16.354 ± 0.008	0.947 ± 0.007	1.160 ± 0.006	0.10	CBF-116, MKKSS-36
214	18.354 ± 0.013	0.621 ± 0.013	1.106 ± 0.013	0.10	CBF-11
228	17.123 ± 0.003	0.685 ± 0.002	0.989 ± 0.001	0.10	CBF-70, CS-C03, MD-47, SBGHS-13
234	19.677 ± 0.025	0.636 ± 0.024	1.066 ± 0.022	0.10	CBF-75
236	18.793 ± 0.008	0.827 ± 0.007	1.030 ± 0.006	0.10	CBF-74, CS-H24
240	20.921 ± 0.060	0.906 ± 0.048	1.366 ± 0.038	0.15	CBF-82
241	17.550 ± 0.003	0.821 ± 0.004	1.032 ± 0.003	0.15	CBF-81, CS-C20, MD-55

^aMeasured on CFH12k CCD image with $r = 4.0''$ aperture.

^bMeasured on CFH12k CCD image with $r = 2.0''$ aperture.

^cMeasured with *UBVRI* PSF Photometry data by Massey et al. (2006). The uncertainties of the values are 0.05.

^dB identifications are from Bedin et al. (2005); CBF identifications from Chandar et al. (1999a, 2001); CS identification from Christian & Schommer (1982); MKKSS identifications from Mochejska et al. (1998); MD identifications are from Melnick & D’Odorico (1978) based on the coordinates given by Ma et al. (2002) ; and S identifications from Sarajedini et al. (2007).